A lab-on-a-chip model of glaucoma

Fatemeh Nafian,†[a] Babak Kamali Doust Azad,†[b] Shahin Yazdani [c,d], Mohammad Javad Rasaee,*[a] and Narsis Daftarian *[c,d]

[a] Department of Medical Biotechnology, Faculty of Medical Sciences, Tarbiat Modares University, Tehran, Iran.

[b] Department of Electronics, School of Electrical and Computer Engineering, Tehran University, Tehran, Iran.

[c] Ocular Tissue Engineering Research Center, Shahid Beheshti University of Medical Sciences, Tehran, Iran.

[d] Ophthalmic Research Center, Shahid Beheshti University of Medical Sciences, Tehran, Iran.

† FN and BKDA has contributed equally to this work and should be considered as co-first authors.

* MJR and ND are co-corresponding authors. All queries and request for reprints should be addressed to MJR. Email: rasaee_m@modares.ac.ir, Tel: +98-21-82884513; FAX: +98-21-82883858.

Abstract

We developed a glaucoma-on-a-chip (GOC) model to evaluate the viability of retinal ganglion cells (RGCs) against high pressure and the potential effect of neuroprotection. A three-layered chip consisting of interconnecting microchannels and culture wells was designed based on simulation of physical parameters. The chip layers were fabricated from poly-methyl methacrylate sheets. Multiple inlet ports allow culture media and gas into the wells under elevated hydrostatic pressure (EHP). The bottom surface of the wells was modified by air plasma and coated with different membranes to model an extracellular microenvironment. The SH-SY5Y neuroblastoma cell line served as model cells to determine the best supporting membrane which was revealed to be PDL/laminin. Thereafter, the study experiments were performed using RGCs obtained from postnatal 5-7 Wistar rats purified by magnetic assisted cell sorting. Flow cytometry and immunocytochemistry assays demonstrated 70% purification for RGCs. The cultured RGCs were exposed to normal (15 mmHg) or elevated pressure (33 mmHg) for 6, 12, 24, 36 and 48 hours, with and without adding brain-derived neurotrophic factor (BDNF) or a novel BDNF mimetic (RNYK). RGC survival rates were 85, 78, 70, 67 and 61 percent under normal pressure versus 40, 22, 18, 12 and 10

percent under high pressure at 6, 12, 24, 36 and 48 hours, respectively (P <0.0001). BDNF and RNYK treatments induced separately an approximate two-fold decrease in the rate of RGC death under both normal and elevated pressures (p <0.01 to 0.0001). This GOC model recapitulated the effects of elevated pressure during relatively short time periods and demonstrated the neuroprotective effects of BDNF and RNYK.

Keywords: Glaucoma; Lab-on-a-chip; microenvironment; elevated hydrostatic pressure; retinal ganglion cell.

1. Introduction

Glaucoma is a collective term used to define a group of neurodegenerative processes affecting the entire visual pathway best distinguished by progressive, irreversible destruction and death of retinal ganglion cells (RGCs). The disease spectrum is estimated to affect more than 100 million people worldwide by the year of 2040 [1]. The primary risk factor for progression and development of glaucoma is elevated intraocular pressure (IOP). IOP is regulated by the balance between aqueous humor secretion into the anterior chamber on one hand and its drainage via the trabecular meshwork (conventional outflow) or the uveoscleral outflow pathways on the other hand [2]. The average value for normal IOP in most population based human studies is 14-17 mmHg with 95% confidence intervals of 10-21 mmHg [3].

Several experimental in vivo glaucoma models have been developed and used for studies on glaucoma mechanisms. These include laser photocoagulation of the Perilimbal region [4], red blood cell or microbeads injection into the anterior chamber [5, 6], Episcleral vein obstruction [7], and Episcleral vein saline injection [8-10]. Without sequential treatments, the duration of IOP elevation is transient in these models. Precise control over IOP elevation is difficult and certain problems may occur; these include intraocular inflammation, irreversible mydriasis, IOP variability, hyphema, reduced visibility of optic discs, corneal opacity, and scleral burns [11, 12]. While in vivo animal models are indispensable to determine what events occur in live organisms, these strategies typically involve poorly defined and uncontrollable factors and the results can be difficult to understand at cellular and molecular levels [13].

Ishikawa et al. designed an ex vivo hydrostatic pressure model which demonstrated better retention of neuron-neuron and neuron-glial interactions in dissected eye cups [14-18]. This model excluded the effects of ischemia and allowed studying of the direct effects of pressure on the retina. Eyecups were sunken to the bottom of a glass cylinders containing different liquid heights. Although ex vivo systems produce reliable results, there are several limitations. For example, the incubation period is limited by the duration of tissue viability because survival factors originating from axonal transport or the bloodstream are eliminated in ex vivo models[13].

To overcome these limitations, in vitro models have been developed using cultured cells in supporting environments to clarify glaucoma mechanisms and appear as valuable tools to evaluate the response of individual cell populations against noxious conditions and novel treatments [19-21]. These models have studied optic nerve head astrocytes, RGCs and other types of retinal cells utilizing pressure loading systems [21-28]. Elevation of pressure constitutes the gold standard to model ocular hypertension in vitro and has gained increasing attention in recent years. Elevated hydrostatic pressure (EHP) systems provide remarkable information on cell apoptosis, elastin synthesis, cell migration, and production of cell adhesion molecules. EHPs have provided new insights into the molecular and cellular mechanisms of glaucoma.

Recently, lab-on-a-chip (LOC) technology has been developed. This approach entails a simpler and smaller analysis platform, resulting in better temporal and spatial control of local cellular microenvironments, passive and active cell handling, less consumption of reagents, faster test results, economizing study logistics and energy savings [29-32]. With the goal of transferring costly laboratory equipment onto small, user-friendly, easily replicable chips, LOC technology has dramatically altered many fields such as medicine, biochemistry, and biotechnology.

The aim of the present study was to design and establish a glaucoma-on-a-chip (GOC) model consisting of an EHP system, coupled to a microculture system using purified primary rat RGCs. To achieve this aim, we designed pressure chips in which HP could be modulated with the added benefits of higher speed, greater precision and finer control than previous EHP systems. We studied RGC survival under normal versus

elevated hydrostatic pressures and also compared survival of these cells when treated with a neuroprotective growth factor (brain-derived neurotrophic factor, BDNF) or a mimicry peptide, named RNYK, as a putative agonist of neurotrophic tyrosine kinase receptor type 2 (NTRK2) [33]. BDNF is a well-known neuroprotectant and a potent therapeutic candidate for neurodegenerative diseases. However, there are several clinical concerns about its therapeutic applications. RNYK as a mimicking small peptide (similar to loop2 of BDNF) is an alternative to circumvent these problems. The RNYK neuroprotective effect has been confirmed with equal efficacy to or even better than BDNF.

2. Material and methods

2.1.Design of a three-layered chip

In order to induce a high pressure environment to simulate glaucomatous conditions, several three-layered EHP models were designed (Fig. 1). A number of morphological parameters were considered including number and location of feeding ports in the top layer (layer A), the shape of micro-channels and wells in the middle layer (layer B), and surface modification for the bottom layer (layer C) of the chip. AutoCAD 2014 was used to design the layers. Some physical parameters including gas concentrations and fluid velocity profile for media at seeding/feeding time were simulated by Comsol Multiphysics 5.2a software employing finite element methods. Two-dimensional incompressible Navier-Stokes equations were used along with the continuity equation to determine the liquid velocity profile of culture media throughout the fluid dynamic field at the seeding and feeding time

$$\nabla \cdot \boldsymbol{u} = 0 \quad (1)$$

$$\rho \boldsymbol{u} \cdot \nabla \boldsymbol{u} = -\nabla p + \mu \nabla^2 \boldsymbol{u} \quad (2)$$

Where **u** is the velocity vector, p is the pressure of injection, ρ is the density of media, and μ is the dynamic viscosity. The no-slip boundary condition was assumed at the walls. Constant velocity was specified at the inlet. The outlet was assumed to be at atmospheric pressure.

After the flow reached a steady-state condition, gas was assumed to be transported only by diffusion so that gas distribution was estimated using Fick's law (FL). Gas was released at the inlet at a specific concentration (C_0), which was monitored after a certain sampling time period. The transient two-dimensional mass transport equation is as follows:

$$\frac{\partial C}{\partial t} + \mathbf{u} \cdot \nabla C = D\nabla^2 C \quad (3)$$

Where C is the gas concentration in the bulk, and D is the diffusion coefficient.

A novel low-cost fabrication method was established to produce the three-layered chip entirely from poly-methyl methacrylate (PMMA, Cho Chen, Company, city, country). PMMA is the most common member of the acrylic family. The optical clarity and ability to resist environmental stress make PMMA ideal for replacing glass in light transmission applications [34]. PMMA biocompatibility has been established through years in medicine and ophthalmology [35].

2.2.Fabrication and testing of the three-layered chip

A laser system (fiber laser, PNC laser Co. Ltd, Tehran, Iran) was used to cut polymerized PMMA sheets of about 10mm thickness for layer B and 2mm for layers A and C. The laser processing system was equipped with a programming system (NC system), an automatic programming combining computer and CAD technology. When using the laser for fabricating channels and wells on PMMA sheet, the laser power and scanning speed were considered as main factors. Several tests were performed to explore the correct correlation between laser power and scanning speed. A 25W laser power and a 300mm/s laser scanning speed were selected to produce main channels and sub-channels on layer B. In addition, 20W and 45W laser power were applied to cut PMMA sheets 10 mm and 2 mm in thickness respectively, at 100 mm/s laser scanning speed to make the wells and ports in layers A and B.

A thermal-solvent method was used to attach the three layers of any single chip. This method is based on dissolving PMMA in a thin layer of a solvent (isopropyl alcohol) between two PMMA substrates at 75 °C for 10 min [36]. Adhesion of PMMA substrates involved the following steps. First, the layers cut by the

121 laser were rinsed in deionized water for 5 minutes to remove tiny debris and dried at 40 °C for 10 minutes
122 in an oven. Next the solvent was added between layers B and C which were aligned and fixed using paper
123 clamps to avoid entrapment of air bubbles between the binding surfaces. The attached sheets were heated
124 and finally treated with air plasma. Radiofrequency discharged plasma was generated by a dinner plasma
125 generator from Dinner CO. at 13.6 MHZ frequency and 20W power for 10 min. The base pressure of the
126 plasma reactor was increased to 0.35 mmHg after gas feeding. After attaching layers B and C, layer A was
127 attached using the same method described above to complete the three-layered chip.

128 2.3.Extracellular microenvironment model on modified PMMA surface

129 SH-SY5Y cell line which is the third sequential sub-clone of the SKN-SH human neuroblastoma cell
130 line was purchased from the Pasteur Institute (Tehran, Iran). These cells phenotypically change from
131 neuronal type (N) to surface adherent type (S) by all-trans-retinoic acid (ATRA) treatment [37]. The cells
132 were seeded at an initial density of 10^4 cells per cm^2 in the wells of the chip, which were pre-coated with
133 one of the following membranes: collagen (0.05 mg ml^{-1}), ploy-D-lysine (PDL)/laminin (0.01 mg ml^{-1}/0.05
134 mg ml^{-1}), gelatin (1 mg ml^{-1}), and a composite nanofiber of polyacrylonitrile (PAN) and polyaniline (PANI),
135 named PAN/PANI. When the cells were approximately 75% confluent, ATRA (Sigma-Aldrich, Vienna,
136 Austria) treatment was performed at a final concentration of 10 μM in Dulbecco's modified Eagle's
137 medium (DMEM) (Gibco-BRL *Life Technologies*, *Grand Island*, NY) supplemented with 2 mM L-
138 glutamine, penicillin (20 U ml^{-1}), streptomycin (20 mg ml^{-1}), and 15% (by volume) Fetal Bovine Serum
139 *(FBS) (Gibco-BRL Life Technologies*) and incubated for 5 days. Cell morphology, density, and distribution
140 were compared among different coating materials.

141 2.4.Purification of RGCs and primary culture in the chip wells

142 Forty-eight hours before the experiment, chip surface was modified using plasma jet and exposed to
143 UV light for 1h to assess successful sterilization. Then, 500 μl of PDL solution (Sigma-Aldrich), 10 μg ml^{-}
144 ^{1} was added to each well for 1h. The wells were washed three times with sterile water and completely dried.
145 The day before the experiment, 500 μl of laminin solution (5 μg ml^{-1}, Sigma-Aldrich) prepared in

146 Neurobasal medium was added to each well and incubated overnight at 37˚C (8% CO2). The
147 laminin/Neurobasal solution was replaced with 500 µl of "retinal ganglion cell media" which was prepared
148 as follows: Neurobasal medium (Gibco-BRL Life Technologies) with 1% bovine serum albumin (BSA,
149 Sigma-Aldrich), sodium selenite (6.7 ng ml^{-1}, Sigma-Aldrich), Insulin-Transferrin-Selenium (ITS-G)
150 (100X) (Thermo Fisher Scientific, Grand Island, New York, USA), progesterone (20 nM; Merck Millipore),
151 B27 Supplement (50X) (Thermo Fisher Scientific), sodium pyruvate (1 mM; Merck Millipore), L-
152 Glutamine (100x) (2 mM; Gibco-BRL Life Technologies), penicillin (20 U ml^{-1}), and streptomycin (20 mg
153 ml^{-1}).

154 In accordance with the regulations of association for research in vision and ophthalmology (ARVO) for
155 animal studies, ten postnatal day's five to seven Wistar rats (Razi Institute, Karaj, Iran) were sacrificed by
156 decapitation and then enucleated. The cornea, lens, and vitreous humor were removed and the retina was
157 gently lifted away using a small spatula. The retinas were stored at room temperature in 4.5 ml Hank's
158 balanced salt solution, Ca2+ and Mg2+ free (HBSS-CMF, Sigma-Aldrich), pH 7.4. Then, 0.5 ml of trypsin
159 (2.5%, Gibco-BRL *Life Technologies*) was added to the tube containing five retinas and incubated in a
160 water bath at 37˚C for 15 min where the tube was gently swirled every 5 min. The HBSS/trypsin solution
161 was replaced by 5 ml of HBSS (containing 50 µl of DNase I 0.4%) and incubated at 37˚C for 5 min. The
162 retina was converted into a cell suspension by triturating and homogenizing the solution without introducing
163 bubbles. The cells were centrifuged at 300g for 5 min and re-suspended in 1ml HBSS containing 0.5 mg
164 ml^{-1} BSA. The cell suspension was filtered through a mesh filter (pore size 40 µm, BD Falcon, Franklin
165 Lakes, NJ) to yield a single cell suspension.

166 For magnetic assisted cell sorting (MACS), a concentration of 10^7 retinal cells per 90 µl of DBPS/BSA
167 buffer (Dulbecco's PBS containing 0.5 mg ml^{-1} BSA) was incubated with 10 µl of the RGC-specific marker
168 CD90.1 microbeads (Miltenyi Biotec, GmbH, and Bergisch Gladbach, Germany) at room temperature for
169 30 min and then washed with 5 ml of DPBS/BSA buffer. The cell suspension was passed through an LS
170 column to hold the micro bead-labelled cells (RGCs) in the magnetic field of a MidiMACS system

171 (Miltenyi Biotec). The adherent RGCs were rinsed with 3 ml of DPBS/BSA buffer to deplete endothelial
172 cells and microglia. The column was removed from the separator and held over a new 15-ml tube. The
173 adhered cells were flushed out by firmly pushing the plunger into the column and counted.

174 2.5.Flow cytometry and immunocytochemistry of RGCs

175 In different isolation steps, cells were stained with mouse anti-CD90.1 antibody (Millipore, Bedford,
176 MA) and goat anti-mouse IgG antibody FITC conjugated (Santa Cruz Biotechnology, Inc., Dallas, USA)
177 as primary and secondary antibodies, respectively. The anti-CD90.1 antibody was added to the cell
178 suspension at a concentration of 0.1 μg per 100 μl for 10^6 cells and incubated at 4˚C for 20 min. The cells
179 were washed three times with PBS buffer and then 100 μl anti-mouse IgG antibody FITC conjugated was
180 added (1:100 dilution) and incubated at room temperature for 30 min in the dark. After 3-times washing,
181 the fluorescence emission intensity was measured using a flow cytometer. FlowJo (Tree Star, Inc., Ashland,
182 OR) was used to exclude dead cells from the analysis based on scatter signals. The number of cells
183 exhibiting CD90.1 were manually counted, and the RGC percentage was calculated by determining the rate
184 of CD90.1-positive cells relative to other ones.

185 Purified RGCs were cultured on a chip pre-coated with PDL/laminin at 37˚C and 8% CO2. After a 3-
186 day culture, RGCs were fixed with cold methanol (-10˚C) for 10 min, dried, and then blocked with 300μl
187 of PBS containing 1% BSA for 20 min at room temperature. The cells were incubated with 10 μl mouse
188 anti-CD90.1 antibody (1:100 dilution) as a primary antibody overnight at 4 °C. RGCs were exposed to goat
189 anti-mouse IgG antibody FITC conjugated as a corresponding fluorescent secondary antibody (1:100
190 dilution) at room temperature for 1 h in the dark. Nuclei were counterstained with 4',6-diamidino-2-
191 phenylindole (DAPI, Thermo Fisher Scientific, Pennsylvania, USA) as a colouring reagent. To determine
192 the expression of specific marker on the RGC surface (CD90.1-positive cells), several random fields were
193 imaged under a fluorescence microscope.

194 2.6.Measurement of Cell Viability

195 RGCs were seeded at an initial density of 10^4 cells per cm2 in two sets of 12-well chips prior to the
196 pressure experiment. RGCs were exposed to high hydrostatic pressures in a time-dependent manner for 6,
197 12, 24, 36 and 48 hours. BDNF (50 ng ml^{-1}; Thermo Fisher Scientific, Waltham, USA) and RNYK peptide
198 (5 ng ml^{-1}) were separately applied to RGCs in one chip under normal and the other elevated hydrostatic
199 pressure. RGCs in control groups did not receive BDNF/RNYK in the same experiments. The chip pressure
200 was checked periodically by tonometer for fluctuations to hold the pressure level constant in each test. Cell
201 viability was measured using 3-(4, 5-dimethylthiazol-2-yl)-2, 5-diphenyltetrazolium bromide (MTT,
202 Sigma-Aldrich) assay for each well in the six groups. MTT solution was added to the media at a final
203 concentration of 0.5 mg ml^{-1} and aspirated from the wells after 4 h. The residual crystals (formazan) were
204 dissolved in dimethyl sulfoxide (DMSO, Sigma-Aldrich) and the absorbance was measured at near 570 nm.
205 These experiments were repeated for at least three times to check the reproducibility of biologic effects.
206 All measured variables were described as mean ±SD.

207 2.7.Statistical Analysis

208 Cell viability in BDNF/RNYK treatment groups was compared to that of untreated controls under
209 normal and elevated pressure. The GraphPad Prism 7.0 statistical software was employed (San Diego,
210 USA). Significance was determined at $p < 0.05$ level using two-way ANOVA with Holm-Sidak's multiple
211 comparison test.

212 **3. Results**

213 3.1.Testing of the three-layered chip

214 The three-layered chip was designed to allow inflow of cell culture media from feeding inlets in layer
215 A into the wells in layer B adjacent to layer C which acts the culture surface at the bottom of the wells (Fig.
216 1). We fabricated stand-alone feeding inlets for each well to let treat culture cells within the wells in an
217 individual manner. We initially devised two feeding ports per well in layer A (the results not shown). The
218 drawback to this design was inappropriate surface tension leading to an uneven distribution of the culture

media. We then shifted to a single feeding port at one extreme of the well and placed a gas inlet on the other extreme to allow uniform liquid distribution. Locating the feeding port at the extreme end of the well reduced shearing stress and avoided cellular detachment and necrosis in the mid-region of the well.

Based on simulation results, a hexagonal (divergent-convergent) well performed better than a rectangular well. If the cells are seeded into a rectangular well, they mainly localize in the central zone due to maximum velocity there influenced by boundary layers related to sidewalls (Fig. 2A, red curve). Whereas, velocity profile became more even in a divergent-convergent input due to the reduction cross section area and mitigation of boundary layer effects (Fig. 2B, blue curve), resulting in a homogeneous flow velocity and cell distribution across the well at the feeding and seeding times, respectively. We designed 12 wells in each chip for simultaneously RGCs treatment with different compounds per well without any mixing of culture media or cells from one well to another via the gas channels during feeding process. The gas channels necessarily had to be interconnected to provide the same level of pressure and gas conditions to all wells within a chip. A single gas inlet was located for each chip which led to two separate main channels with six branching sub-channels (Fig. 2C).

The bottom surface of the wells (layer C) were treated by air plasma to chemical modification and functionalization. This surface treatment increases surface roughness, amount of oxygen atoms, and functional hydrophilic groups (and as a result the number of polar interactions), especially the electron-donor parameters. These modifications enhance cellular adhesion which is fundamental for cell growth, migration, and differentiation.

3.2.Extracellular microenvironment model on modified PMMA surface

ATRA was added to the culture media to differentiate SH-SY5Y neuroblastoma cells into more mature, neuron-like cells. ATRA is a powerful growth inhibitor but promotes normal cellular differentiation. This low cost procedure is easily performed as compared to primary neuronal culture and may generate a homogenous neuronal cell population. The morphology and distribution of neuron-like cells were distinguished by phase-contrast microscopy (Fig. 3A). Untreated neuroblastoma cells possess large and flat

244 cell bodies, however neuron-like cells have branching neuronal networks with smaller and round cell
245 bodies. The neuron-like cells were cultured onto plasma-treated PMMA with different membrane coating
246 to model the extracellular microenvironment in vitro (Fig. 3B).

247 The cellular density was significantly more ordered with PDL/laminin coating as compared to gelatin
248 and collagen membranes, PAN/PANI nanocomposite or non-modified surface (negative control). The SH-
249 SY5Y exhibited better differentiated morphology and more regular pattern of growth on the PDL/laminin
250 membrane. Furthermore, the PDL/laminin membrane induced neurite elongation and branching, while
251 other membranes increased cell aggregation, reminiscent of the aggregation commonly observed in
252 undifferentiated cultures. Due to these reasons, we selected PDL/laminin surface coating for cell culture
253 purposes in the following experiments.

254 3.3.Characterization of RGCs

255 The steps of RGC isolation by MACS technique are summarized in Fig. 4A. After isolation, flow
256 cytometry showed high purity of RGCs, in which the percentage of RGCs was calculated by determining
257 the ratio of CD90.1-positive cells (Fig. 4B). Isolation of RGCs was initially performed using a mesh filter
258 according to RGC cell size (>40μm) to increase their population from a baseline of 19.8% in the single-
259 cell retinal suspension to 37.4%. In the later stage MACS isolated RGCs according to CD90.1 surface
260 marker in a 'yes or no' decision manner up to 70.4% purification. The RGCs exhibiting CD90.1 were also
261 characterized using immunocytochemistry assay by above-mentioned antibodies and counterstaining with
262 DAPI (Fig. 5).

263 The RGCs were identified by their morphology and immunofluorescence staining characteristics.
264 Dendrites and axons typically appear at opposing poles of the neuronal cell. On non-modified PMMA
265 surface, RGCs tend to form cell clusters with small to media round cell bodies with few extended fine
266 neurites after a 10-day culture. The majority of RGCs on the modified PMMA surface exhibited uniform
267 and round cell bodies, with neurites extending to connect to one other. At day 10, the cells developed a
268 complex dendritic network with numerous neurites and branches (Table 1).

Table 1. Morphological changes of primary RGCs at different time intervals on modified and non-modified PMMA surfaces before the pressure experiment. Scale bar= 50 µm.

Time Intervals	Culture on a modified PMMA surface	Culture on non-modified PMMA surface
1 DAY	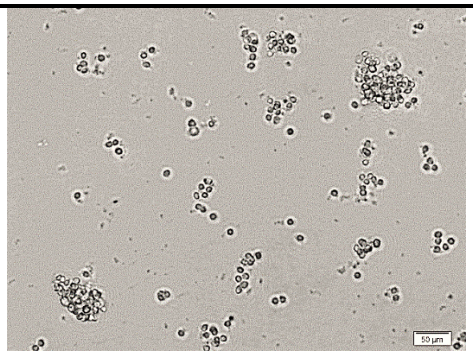	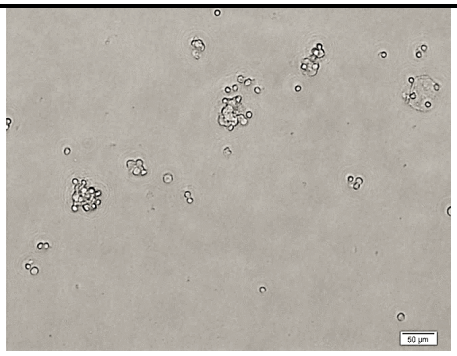
3 DAY	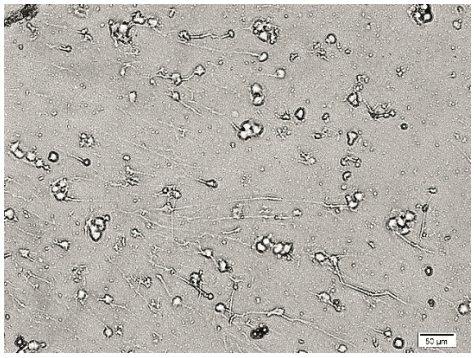	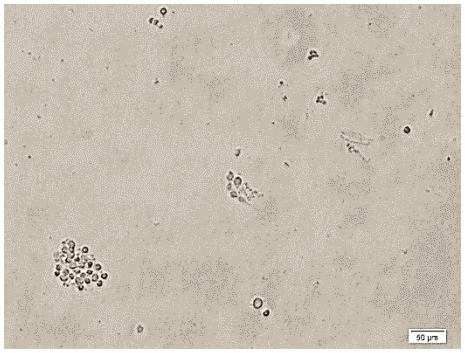
10 DAY	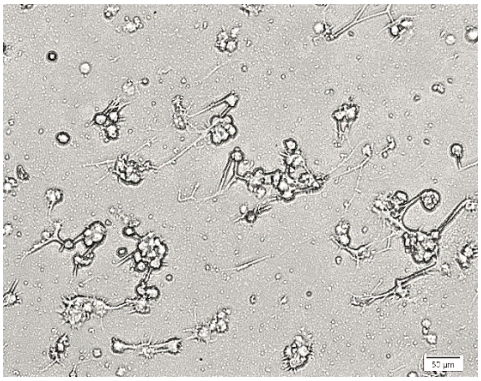	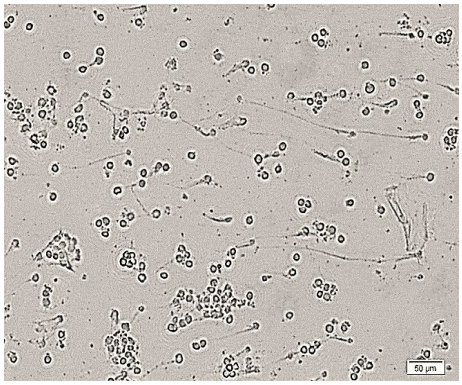
13 DAY	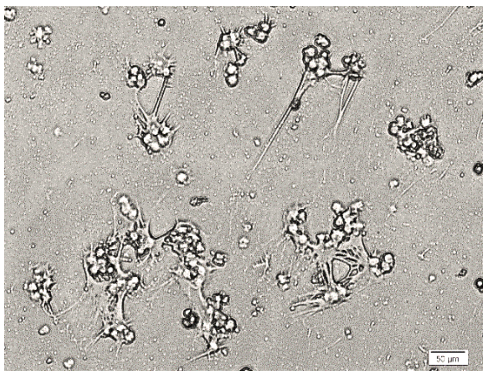	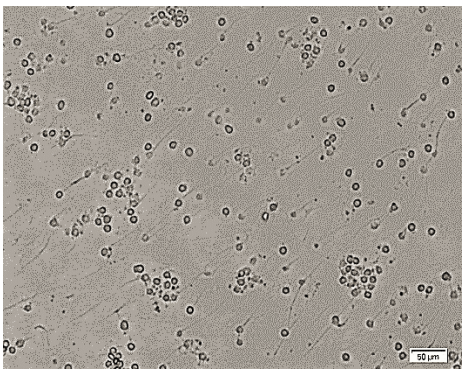

272 3.4.Measurement of Cell Viability

273 One set of the chips was connected to a gas tank to apply elevated pressure at 33 mmHg,
274 while another chip were exposed to normal pressure at 15 mmHg. As summarized in Figure 6,
275 the EHP system consisted of a compressed 8% CO2/92% air gas tank, which was placed just
276 outside the incubator and adjusted with both regulators for normal and ultra-low delivery
277 pressure. Polyurethane hoses (4/8" ID) were used to feed the gas mixture into the pressure chip
278 through a port at the back of the incubator. A digital pressure gauge (Ashcroft, DG25; 0.5% of
279 0-15psi span accuracy, ±0.1 mmHg sensitivity; relative to atmospheric pressure) was used to
280 monitor the input pressure value. Pneumatic fittings were placed into the inlet/outlet circuits to
281 provide tight control over gas flow. During loading, the pressure was also monitored by a
282 sensor in the chip and kept at the 33 mm Hg with the accuracy of ±0.1 mmHg (data not shown).

283 Untreated RGCs decreased in a time-dependent manner when elevated hydrostatic pressure
284 was applied in the chip (Fig. 7A). From 6h of EHP onwards, a significant difference was
285 observed in cell survival as compared to control cells under normal hydrostatic pressure. Cell
286 viability results showed 85, 78, 70, 67 and 61 percent cell survival under normal pressure versus
287 40, 22, 18, 12 and 10 percent cell survival under high pressure at 6, 12, 24, 36 and 48 hours (p
288 <0.0001), respectively. BDNF-treated RGCs demonstrated better cell survival with or without
289 elevated pressure as compared to untreated cells. BDNF-treated RGCs showed 92, 89, 88, 83
290 and 80 percent viability under normal pressure compared to 72, 67, 64, 60 and 53 percent under
291 high pressure at 6 ($p = 0.0198$), 12 ($p = 0.0022$), 24 ($p = 0.0004$), 36 ($p < 0.0001$) and 48 (p
292 <0.0001) hours, respectively (Fig. 7B). RNYK provided slightly more stability than BDNF
293 over time. RNYK-treated RGCs showed 94, 93, 89, 87 and 86 percent viability under normal
294 pressure compared to 67, 66, 63, 60 and 58 percent under high pressure at 6, 12, 24, 36 and 48
295 hours ($p < 0.0001$), respectively (Fig. 7C). BDNF and RNYK treatments induced separately an

296 approximate two-fold decrease in RGC death rates as compared to untreated cells under both
297 normal and elevated pressure condition.

298 ## 4. Discussion

299 Pressure chambers are important tools to study the influence of elevated pressure on
300 individual cell types [38]. Prior to employing animal models, they allow the assessment of pre-
301 defined experimental conditions and evaluation of specific variables contributing to cell
302 survival. Over the past two decades, various studies have reported significant changes in the
303 behaviour of different cells following the application of hydrostatic pressure [22, 26, 39-47].
304 These changes include increased apoptosis, changes in cell morphology and gene expression.
305 Neuronal cells including PC12 [48, 49] and RGC-5 cell lines [23, 50-53], primary cultures of
306 RGC [54, 55], optic nerve head astrocytes [24, 27, 28, 56-61], Müller cells [62-64], or
307 microglial cells [65-67], and more complex preparations such as organotypic co-cultures of the
308 retinal cells [25, 68, 69] or eye cup preparations [15, 17, 70, 71] have been exposed to elevated
309 pressure.

310 In the vast majority of glaucoma patients, IOP levels may vary from 20 to 35 mmHg.
311 Several in vitro glaucoma models have been developed to improve the accuracy and
312 repeatability of experimental conditions in this pressure range. Pressurized chamber is the most
313 commonly used model established by Kosnosky et al. (1995) and modified by Agar at al.
314 (2000) to investigate cellular mechanisms [49, 72]. In this system, a mixture of humidified gas
315 is injected through a pressure regulator into a glass macro-chamber with ±1.5 mmHg variation.
316 Studies using this chamber have indicated that exposure of RGC-5 cells to 30, 50, or 100 mmHg
317 for 72, 6, or 2 h, respectively, triggers apoptosis via oxidative stress and mitochondrial
318 dysfunction, similar to the human condition when comparing acute glaucoma (100 mmHg)
319 with chronic glaucoma (30 mmHg) [23, 50-52, 73-75]. The second important model is a

320 hydraulic pressurizing chamber introduced by Parkkinen et al. (1993), which compressed the
321 internal gas phase using a hydraulic system [76]. Tezel and wax (2000) used this device to
322 expose RGCs to 50 mmHg for 72 h and promote neurodegeneration [22, 25].

323 In the present study, we designed a glaucoma-on-a-chip system that provides continuous
324 hydrostatic pressure with ±0.1 mmHg variation under a temperature-controlled environment.
325 Our system was custom-made in agree with the pressurized chamber approach, thus, several
326 conditions and confounding factors were carefully simulated, validated or controlled
327 beforehand. They consisted of fluid velocity fields, alterations in gas composition, temperature
328 and osmolarity to design a more stable and adjustable experiment compared to prior in vitro
329 studies. Our results indicated that glaucoma-on-a-chip can simulate glaucomatous conditions
330 only when provided with a suitable microenvironment for cell-to-cell communication of RGCs.
331 Accordingly, the PMMA surface was modified by air plasma and a thin layer of PDL/laminin
332 to form a continuous surface of mechanical properties and uniform chemistry leading to a
333 homogenous cell distribution. Furthermore, the evaluation of cellular mechanisms requires
334 isolation and culture of primary RGCs. Early postnatal tissues were used to optimize RGC
335 viability in primary cell cultures due to the limited yield and the typically post-mitotic feature
336 of these neurons in the next state. The use of RGCs in cultures on chips allowed examining a
337 direct in vitro situation in which retinal cells maintain their microarchitecture.

338 Most reports investigating the degenerative effect of chronic IOP elevation have used
339 pressures ranging from 30 mmHg (for 72 h) to 100 mmHg (for 2 h), as already described. In
340 the present study, we exposed RGCs to 33 mmHg (elevated hydrostatic pressure, EHP) or 15
341 mmHg (normal pressure) for 6, 12, 24, 36 and 48 hours, with and without adding
342 neuroprotective agents. Accordingly, cell survival of primary rat RGCs was evaluated under
343 four different experimental conditions simulating the high pressure glaucoma (untreated RGCs
344 under EHP), normal-tension glaucoma (BDNF deprived RGCs under normal pressure),

345 neuroprotective-treated glaucoma (BDNF/RNYK treated RGCs under EHP), and normal
346 conditions (BDNF-treated RGCs under normal pressure). Our results demonstrated that BDNF
347 can maintain neuronal viability despite high pressure. According to cell survival patterns and
348 rates, the neuroprotective influence of BDNF seems to cancel the detrimental effect of elevated
349 pressure. This suggests that the negative impact of neurotrophin deprivation can be compared
350 to the insult of high pressure. This may be equivalent to the observation that failure of axonal
351 transport of neurotrophins in glaucoma triggers RGC degeneration and that retinal cells
352 essentially require neurotrophic input from target neurons in the brain.[77, 78]

353 This previously confirmed that RNYK can mimic BDNF activities in vitro at an optimum
354 concentration of 5 ng ml^{-1}. RNYK prevented neuronal degeneration of ATRA-treated SH-
355 SY5Y with equal efficacy to or even better than BDNF at 50 ng ml^{-1} [33]. In the current study,
356 RNYK indicated a neuroprotective effect comparable to BDNF on primary RGCs under both
357 normal and elevated pressures. In light of the findings obtained, the identified peptidomimetic
358 compound is significant as a promising neuroprotective agent for glaucoma treatment. Also,
359 small size of RNYK might be an advantage for drug design and synthesis in future. It is clear
360 that in vitro models may never substitute animal studies, but they are important tools in
361 preclinical studies. Glaucoma-on-a-chip offers the advantages of allowing controlled
362 experimental conditions, preliminary targeting of a specific cell type or pathway involved in
363 glaucomatous damage. More studies are needed to develop models to study RGC
364 neurodegeneration and neuroprotection by putative agents such as neurotrophins, peptides, and
365 other small molecules prior to assessment in animal models.

366 **Conflicts of interest**

367 The authors declare that no conflict of interest exists.

Acknowledgements

We are thankful to Dr. S Gharavi (Alzahra University, Tehran, Iran) and Dr. N K Tafreshi (Moffitt Cancer Center and Research Institute, Florida, USA) for technical support.

References

[1] Y.-C. Tham, X. Li, T.Y. Wong, H.A. Quigley, T. Aung, C.-Y. Cheng, Global prevalence of glaucoma and projections of glaucoma burden through 2040: a systematic review and meta-analysis, Ophthalmology 121 (11) (2014) 2081-2090.
[2] L.A. Levin, S.F. Nilsson, J. Ver Hoeve, S. Wu, P.L. Kaufman, A. Alm, Adler's Physiology of the Eye E-Book, Elsevier Health Sciences 2011.
[3] J. Rieck, The pathogenesis of glaucoma in the interplay with the immune system, Invest. Ophthalmol. Vis. Sci. 54 (3) (2013) 2393-2409.
[4] D. Gaasterland, C. Kupfer, Experimental glaucoma in the rhesus monkey, Invest. Ophthalmol. Vis. Sci. 13 (6) (1974) 455-457.
[5] H.A. Quigley, E.M. Addicks, Chronic experimental glaucoma in primates. I. Production of elevated intraocular pressure by anterior chamber injection of autologous ghost red blood cells, Invest. Ophthalmol. Vis. Sci. 19 (2) (1980) 126-136.
[6] N. Kalvin, D. Hamasaki, J. Gass, Experimental glaucoma in monkeys: I. Relationship between intraocular pressure and cupping of the optic disc and cavernous atrophy of the optic nerve, Arch. Ophthalmol. 76 (1) (1966) 82-93.
[7] M.V. Fedorchak, I.P. Conner, C.A. Medina, J.B. Wingard, J.S. Schuman, S.R. Little, 28-day intraocular pressure reduction with a single dose of brimonidine tartrate-loaded microspheres, Exp. Eye Res. 125 (2014) 210-216.
[8] S. Shareef, E. Garcia-Valenzuela, A. Salierno, J. Walsh, S. Sharma, Chronic ocular hypertension following episcleral venous occlusion in rats, Exp. Eye Res. 61 (3) (1995) 379-382.
[9] J.C. Morrison, C. Moore, L.M. Deppmeier, B.G. Gold, C.K. Meshul, E.C. Johnson, A rat model of chronic pressure-induced optic nerve damage, Exp. Eye Res. 64 (1) (1997) 85-96.
[10] E. Vecino, S.C. Sharma, Glaucoma animal models, Glaucoma-Basic and Clinical Concepts, InTech. 15 (2011) 320-334.
[11] T.V. Johnson, S.I. Tomarev, Rodent models of glaucoma, Brain Res. Bull. 81 (2) (2010) 349-358.
[12] M. Rudzinski, H.U. Saragovi, Glaucoma: validated and facile in vivo experimental models of a chronic neurodegenerative disease for drug development, Current Medicinal Chemistry-Central Nervous System Agents 5 (1) (2005) 43-49.
[13] M. Ishikawa, T. Yoshitomi, C.F. Zorumski, Y. Izumi, Experimentally induced mammalian models of glaucoma, BioMed research international 2015 (2015) 1-11.
[14] M. Ishikawa, T. Yoshitomi, D.F. Covey, C.F. Zorumski, Y. Izumi, TSPO activation modulates the effects of high pressure in a rat ex vivo glaucoma model, Neuropharmacology 111 (2016) 142-159.
[15] M. Ishikawa, T. Yoshitomi, C.F. Zorumski, Y. Izumi, Effects of acutely elevated hydrostatic pressure in a rat ex vivo retinal preparation, Invest. Ophthalmol. Vis. Sci. 51 (12) (2010) 6414-6423.
[16] M. Ishikawa, T. Yoshitomi, C.F. Zorumski, Y. Izumi, Neurosteroids are endogenous neuroprotectants in an ex vivo glaucoma model, Invest. Ophthalmol. Vis. Sci. 55 (12) (2014) 8531-8541.
[17] M. Ishikawa, T. Yoshitomi, C.F. Zorumski, Y. Izumi, Downregulation of glutamine synthetase via GLAST suppression induces retinal axonal swelling in a rat ex vivo hydrostatic pressure model, Invest. Ophthalmol. Vis. Sci. 52 (9) (2011) 6604-6616.
[18] M. Ishikawa, T. Yoshitomi, D.F. Covey, C.F. Zorumski, Y. Izumi, Additive neuroprotective effects of 24 (S)-hydroxycholesterol and allopregnanolone in an ex vivo rat glaucoma model, Sci. Rep. 8 (1) (2018) 1-15.
[19] N. Maurya, N.R. Agarwal, I. Ghosh, Low-dose rotenone exposure induces early senescence leading to late apoptotic signaling cascade in human trabecular meshwork (HTM) cell line: An in vitro glaucoma model, Cell Biol. Int. 40 (1) (2016) 107-120.
[20] M. Dai, Q. Zhang, Z. Zheng, J. Wang, Retinal ganglion cell-conditioned medium and surrounding pressure alters gene expression and differentiation of rat retinal progenitor cells, Mol. Med. Report. 17 (5) (2018) 7177-7183.
[21] Y. Lei, S. Rajabi, R.M. Pedrigi, D.R. Overby, A.T. Read, C.R. Ethier, In vitro models for glaucoma research: effects of hydrostatic pressure, Invest. Ophthalmol. Vis. Sci. 52 (9) (2011) 6329-6339.
[22] M.B. Wax, G. Tezel, S. Kobayashi, M.R. Hernandez, Responses of different cell lines from ocular tissues to elevated hydrostatic pressure, Br. J. Ophthalmol. 84 (4) (2000) 423-428.
[23] A. Agar, S. Li, N. Agarwal, M.T. Coroneo, M.A. Hill, Retinal ganglion cell line apoptosis induced by hydrostatic pressure, Brain Res. 1086 (1) (2006) 191-200.

[24] M. Salvador-Silva, S. Aoi, A. Parker, P. Yang, P. Pecen, M.R. Hernandez, Responses and signaling pathways in human optic nerve head astrocytes exposed to hydrostatic pressure in vitro, Glia 45 (4) (2004) 364-377.
[25] G. Tezel, M.B. Wax, Increased production of tumor necrosis factor-α by glial cells exposed to simulated ischemia or elevated hydrostatic pressure induces apoptosis in cocultured retinal ganglion cells, J. Neurosci. 20 (23) (2000) 8693-8700.
[26] M.R. Hernandez, J.D. Pena, J.A. Selvidge, M. Salvador-Silva, P. Yang, Hydrostatic pressure stimulates synthesis of elastin in cultured optic nerve head astrocytes, Glia 32 (2) (2000) 122-136.
[27] C.S. Ricard, S. Kobayashi, J.D. Pena, M. Salvador-Silva, O. Agapova, M.R. Hernandez, Selective expression of neural cell adhesion molecule (NCAM)-180 in optic nerve head astrocytes exposed to elevated hydrostatic pressure in vitro, Molecular brain research 81 (1-2) (2000) 62-79.
[28] P. Yang, O. Agapova, A. Parker, W. Shannon, P. Pecen, J. Duncan, M. Salvador-Silva, M.R. Hernandez, DNA microarray analysis of gene expression in human optic nerve head astrocytes in response to hydrostatic pressure, Physiological genomics 17 (2) (2004) 157-169.
[29] J. El-Ali, P.K. Sorger, K.F. Jensen, Cells on chips, Nature 442 (7101) (2006) 403-411.
[30] E.W. Esch, A. Bahinski, D. Huh, Organs-on-chips at the frontiers of drug discovery, Nature reviews Drug discovery 14 (4) (2015) 248–260.
[31] D.E. Ingber, Reverse engineering human pathophysiology with organs-on-chips, Cell 164 (6) (2016) 1105-1109.
[32] A. Balijepalli, V. Sivaramakrishan, Organs-on-chips: research and commercial perspectives, Drug discovery today 22 (2) (2017) 397-403.
[33] F. Nafian, M. Rasaee, S. Yazdani, N. Daftarian, Z. Soheili, B. Kamali Doust Azad, Peptide selected by phage display increases survival of SH-SY5Y neurons comparable to brain-derived neurotrophic factor, J. Cell. Biochem. 120 (3) (2018) 1-11.
[34] C. Henkel, Design Guide for Bonding Plastics, Henkel Corporation 6 (2011) 1-100.
[35] R.Q. Frazer, R.T. Byron, P.B. Osborne, K.P. West, PMMA: an essential material in medicine and dentistry, J. Long. Term Eff. Med. Implants 15 (6) (2005) 629-639.
[36] A. Bamshad, A. Nikfarjam, H. Khaleghi, A new simple and fast thermally-solvent assisted method to bond PMMA–PMMA in micro-fluidics devices, Journal of Micromechanics and Microengineering 26 (6) (2016) 1-12.
[37] J. Kovalevich, D. Langford, Considerations for the use of SH-SY5Y neuroblastoma cells in neurobiology, Neuronal Cell Culture, Springer 2013 (2013) 9-21.
[38] I. Aires, A. Ambrósio, A. Santiago, Modeling Human Glaucoma: Lessons from the in vitro Models, Ophthalmic Res. 57 (2) (2017) 77-86.
[39] O. Tokunaga, T. Watanabe, Properties of endothelial cell and smooth muscle cell cultured in ambient pressure, In Vitro Cell. Dev. Biol. 23 (8) (1987) 528-534.
[40] A.D. Acevedo, S.S. Bowser, M.E. Gerritsen, R. Bizios, Morphological and proliferative responses of endothelial cells to hydrostatic pressure: role of fibroblast growth factor, J. Cell. Physiol. 157 (3) (1993) 603-614.
[41] O. Thoumine, R.M. Nerem, F.R. Girard, Oscillatory shear stress and hydrostatic pressure modulate cell-matrix attachment proteins in cultured endothelial cells, In Vitro Cellular & Developmental Biology-Animal 31 (1) (1995) 45-54.
[42] S. Salwen, D. Szarowski, J. Turner, R. Bizios, Three-dimensional changes of the cytoskeleton of vascular endothelial cells exposed to sustained hydrostatic pressure, Med. Biol. Eng. Comput. 36 (4) (1998) 520-527.
[43] E.A. Schwartz, R. Bizios, M.S. Medow, M.E. Gerritsen, Exposure of human vascular endothelial cells to sustained hydrostatic pressure stimulates proliferation: involvement of the αv integrins, Circ. Res. 84 (3) (1999) 315-322.
[44] K.M. Haberstroh, M. Kaefer, A.B. Retik, M.R. Freeman, R. Bizios, The effects of sustained hydrostatic pressure on select bladder smooth muscle cell functions, The Journal of urology 162 (6) (1999) 2114-2118.
[45] Y. Sugaya, N. Sakamoto, T. Ohashi, M. Sato, Elongation and random orientation of bovine endothelial cells in response to hydrostatic pressure: comparison with response to shear stress, JSME International Journal Series C Mechanical Systems, Machine Elements and Manufacturing 46 (4) (2003) 1248-1255.
[46] T. Ohashi, Y. Sugaya, N. Sakamoto, M. Sato, Hydrostatic pressure influences morphology and expression of VE-cadherin of vascular endothelial cells, J. Biomech. 40 (11) (2007) 2399-2405.
[47] Y. Kao, J. Jheng, H. Pan, W. Liao, C. Lee, P. Kuo, Elevated hydrostatic pressure enhances the motility and enlarges the size of the lung cancer cells through aquaporin upregulation mediated by caveolin-1 and ERK1/2 signaling, Oncogene 36 (6) (2017) 863-874.
[48] L. Tök, M. Nazıroğlu, A.C. Uğuz, Ö. Tök, Elevated hydrostatic pressures induce apoptosis and oxidative stress through mitochondrial membrane depolarization in PC12 neuronal cells: A cell culture model of glaucoma, Journal of Receptors and Signal Transduction 34 (5) (2014) 410-416.
[49] A. Agar, S.S. Yip, M.A. Hill, M.T. Coroneo, Pressure related apoptosis in neuronal cell lines, J. Neurosci. Res. 60 (4) (2000) 495-503.
[50] W.-K. Ju, Q. Liu, K.-Y. Kim, J.G. Crowston, J.D. Lindsey, N. Agarwal, M.H. Ellisman, G.A. Perkins, R.N. Weinreb, Elevated hydrostatic pressure triggers mitochondrial fission and decreases cellular ATP in differentiated RGC-5 cells, Invest. Ophthalmol. Vis. Sci. 48 (5) (2007) 2145-2151.
[51] W.-K. Ju, K.-Y. Kim, J.D. Lindsey, M. Angert, A. Patel, R.T. Scott, Q. Liu, J.G. Crowston, M.H. Ellisman, G.A. Perkins, Elevated hydrostatic pressure triggers release of OPA1 and cytochrome C, and induces apoptotic cell death in differentiated RGC-5 cells, Mol. Vis. 15 (2009) 120-134.
[52] B. Liu, X. Ma, D. Guo, Y. Guo, N. Chen, H. Bi, Neuroprotective effect of alpha-lipoic acid on hydrostatic pressure-induced damage of retinal ganglion cells in vitro, Neurosci. Lett. 526 (1) (2012) 24-28.

[53] J.K. Lee, S. Lu, A. Madhukar, Real-time dynamics of Ca2+, caspase-3/7, and morphological changes in retinal ganglion cell apoptosis under elevated pressure, PLoS One 5 (10) (2010) e13437.
[54] R.M. Sappington, M. Chan, D.J. Calkins, Interleukin-6 protects retinal ganglion cells from pressure-induced death, Invest. Ophthalmol. Vis. Sci. 47 (7) (2006) 2932-2942.
[55] S.-H. Zhang, F.-J. Gao, Z.-M. Sun, P. Xu, J.-Y. Chen, X.-H. Sun, J.-H. Wu, High pressure-induced mtDNA alterations in retinal ganglion cells and subsequent apoptosis, Front. Cell. Neurosci. 10 (2016) 254-264.
[56] M. Salvador-Silva, C.S. Ricard, O.A. Agapova, P. Yang, M.R. Hernandez, Expression of small heat shock proteins and intermediate filaments in the human optic nerve head astrocytes exposed to elevated hydrostatic pressure in vitro, J. Neurosci. Res. 66 (1) (2001) 59-73.
[57] B. Liu, A.H. Neufeld, Nitric oxide synthase-2 in human optic nerve head astrocytes induced by elevated pressure in vitro, Arch. Ophthalmol. 119 (2) (2001) 240-245.
[58] G. Tezel, M.R. Hernandez, M.B. Wax, In vitro evaluation of reactive astrocyte migration, a component of tissue remodeling in glaucomatous optic nerve head, Glia 34 (3) (2001) 178-189.
[59] B. Liu, A.H. Neufeld, Activation of epidermal growth factor receptor signals induction of nitric oxide synthase-2 in human optic nerve head astrocytes in glaucomatous optic neuropathy, Neurobiol. Dis. 13 (2) (2003) 109-123.
[60] H. Miao, A.W. Crabb, M.R. Hernandez, T.J. Lukas, Modulation of factors affecting optic nerve head astrocyte migration, Invest. Ophthalmol. Vis. Sci. 51 (8) (2010) 4096-4103.
[61] A. Mandal, M. Shahidullah, N.A. Delamere, Hydrostatic pressure–induced release of stored calcium in cultured rat optic nerve head astrocytes, Invest. Ophthalmol. Vis. Sci. 51 (6) (2010) 3129-3138.
[62] J. Yu, Y. Zhong, Y. Cheng, X. Shen, J. Wang, Y. Wei, Effect of high hydrostatic pressure on the expression of glutamine synthetase in rat retinal Müller cells cultured in vitro, Exp. Ther. Med. 2 (3) (2011) 513-516.
[63] J. Yu, C. Chen, J. Wang, Y. Cheng, Q. Wu, Y. Zhong, X. Shen, In vitro effect of adenosine on the mRNA expression of Kir 2.1 and Kir 4.1 channels in rat retinal Müller cells at elevated hydrostatic pressure, Exp. Ther. Med. 3 (4) (2012) 617-620.
[64] J. Yu, Y. Zhong, X. Shen, Y. Cheng, J. Qi, J. Wang, In vitro effect of adenosine A2A receptor antagonist SCH 442416 on the expression of glutamine synthetase and glutamate aspartate transporter in rat retinal Müller cells at elevated hydrostatic pressure, Oncol. Rep. 27 (3) (2012) 748-752.
[65] R.M. Sappington, D.J. Calkins, Pressure-induced regulation of IL-6 in retinal glial cells: involvement of the ubiquitin/proteasome pathway and NFκB, Invest. Ophthalmol. Vis. Sci. 47 (9) (2006) 3860-3869.
[66] M.H. Madeira, F. Elvas, R. Boia, F.Q. Gonçalves, R.A. Cunha, A.F. Ambrósio, A.R. Santiago, Adenosine A 2A R blockade prevents neuroinflammation-induced death of retinal ganglion cells caused by elevated pressure, J. Neuroinflammation 12 (1) (2015) 115-128.
[67] R.M. Sappington, D.J. Calkins, Contribution of TRPV1 to microglia-derived IL-6 and NFκB translocation with elevated hydrostatic pressure, Invest. Ophthalmol. Vis. Sci. 49 (7) (2008) 3004-3017.
[68] A. Osborne, A. Aldarwesh, J.D. Rhodes, D.C. Broadway, C. Everitt, J. Sanderson, Hydrostatic pressure does not cause detectable changes in survival of human retinal ganglion cells, PLoS One 10 (1) (2015) 1-14.
[69] M. Obazawa, Y. Mashima, N. Sanuki, S. Noda, J. Kudoh, N. Shimizu, Y. Oguchi, Y. Tanaka, T. Iwata, Analysis of porcine optineurin and myocilin expression in trabecular meshwork cells and astrocytes from optic nerve head, Invest. Ophthalmol. Vis. Sci. 45 (8) (2004) 2652-2659.
[70] X. Zhang, A. Li, J. Ge, D. Reigada, A.M. Laties, C.H. Mitchell, Acute increase of intraocular pressure releases ATP into the anterior chamber, Exp. Eye Res. 85 (5) (2007) 637-643.
[71] D. Reigada, W. Lu, M. Zhang, C.H. Mitchell, Elevated pressure triggers a physiological release of ATP from the retina: possible role for pannexin hemichannels, Neuroscience 157 (2) (2008) 396-404.
[72] W. Kosnosky, B. Tripathi, R. Tripathi, An in-vitro system for studying pressure effects on growth, morphology, and biochemical aspects of trabecular meshwork cells, Invest. Ophthalmol. Vis. Sci., Lippincott-Raven Publ 227 East Washington Square, Philadelphia, 36 (1995) 731-731.
[73] Q. Liu, W.-K. Ju, J.G. Crowston, F. Xie, G. Perry, M.A. Smith, J.D. Lindsey, R.N. Weinreb, Oxidative stress is an early event in hydrostatic pressure–induced retinal ganglion cell damage, Invest. Ophthalmol. Vis. Sci. 48 (10) (2007) 4580-4589.
[74] L. Shang, J.-F. Huang, W. Ding, S. Chen, L.-X. Xue, R.-F. Ma, K. Xiong, Calpain: a molecule to induce AIF-mediated necroptosis in RGC-5 following elevated hydrostatic pressure, BMC Neurosci. 15 (1) (2014) 63.
[75] W.-K. Ju, K.-Y. Kim, J.D. Lindsey, M. Angert, A. Patel, R.T. Scott, Q. Liu, J.G. Crowston, M.H. Ellisman, G.A. Perkins, Elevated hydrostatic pressure triggers release of OPA1 and cytochrome C, and induces apoptotic cell death in differentiated RGC-5 cells, Mol. Vis. 15 (2009) 120-134.
[76] J. Parkkinen, J. Ikonen, M. Lammi, J. Laakkonen, M. Tammi, H. Helminen, Effects of cyclic hydrostatic pressure on proteoglycan synthesis in cultured chondrocytes and articular cartilage explants, Arch. Biochem. Biophys. 300 (1) (1993) 458-465.
[77] R.W. Nickells, The cell and molecular biology of glaucoma: mechanisms of retinal ganglion cell death, Invest. Ophthalmol. Vis. Sci. 53 (5) (2012) 2476-2481.
[78] A. Baltmr, J. Duggan, S. Nizari, T.E. Salt, M.F. Cordeiro, Neuroprotection in glaucoma–is there a future role?, Exp. Eye Res. 91 (5) (2010) 554-566.

552 Figure 1. Schematic of a designed chip in AutoCAD software. (A) Three-dimensional design
553 of layers A (1), B (2), and C (3) containing 12 wells (4), feeding ports (5), and microchannels
554 (6), 2 main channels (7) and 1 single gas inlet (8). Layer A consisted of one feeding port per
555 well and one main gas inlet. Layer B involved 12 hexagonal wells and microchannels. Layer
556 C provided a surface area for cell cultures. Layers were fabricated (B) and assembled (C) to
557 establish a complete chip.

558 Figure 2. Estimated velocity profiles and gas concentration by Comsol Multiphysics software.
559 (A) An entrance region was observed where the upstream flow entered the rectangular well.
560 The boundary layer increased downstream, delayed the axial flow at the wall and accelerated
561 the core flow in the center by maintaining the same flow rate. (B) The velocity profile became
562 more even across the hexagonal well by straitening the walls at the entrance region and
563 reducing the boundary layers at downstream (C) Gas concentration slightly changed throughout
564 the main channels, sub-channels, and wells.

565 Figure 3. Phase contrast images of SH-SY5Y cells. Scale bars 50 μm. (A) Cells phenotypically
566 changed from N-type to S-type by ATRA treatment. (B) Relatively greater number of
567 differentiated cells oriented and aligned on different membranes compared to the naked surface
568 as a negative control. PDL/laminin provided a physiologically optimal environment for
569 neuronal adhesion and expansion.

570 Figure 4. Purification of primary rat RGCs. (A) Retinal cells were isolated and converted into
571 a cell suspension by triturating. The cell suspension was filtered through a mesh filter (>40
572 μm) to yield a single cell suspension. For magnetic assisted cell sorting (MACS), the single
573 cell suspension was incubated with the RGC-specific marker CD90.1 microbeads and passed
574 through an LS column to hold the micro bead-labelled cells (RGCs) in the magnetic field. The
575 adherent RGCs were rinsed to deplete endothelial cells and microglia. The column was

576 removed from the separator and the adhered cells were flushed out by firmly pushing the
577 plunger into the column and counted. (B) Flow cytometry results showed that CD90.1+ cells
578 were more purified after positive selection using MACS (orang, 70.4% purity) rather than mesh
579 filtration (blue, 37.4%) and initial retinal single-cell suspension (red, 19.8%).

580 Figure 5. CD90.1 immunostaining of isolated rat RGCs by MACS. (A) After 3-day normal
581 culture, RGCs continued to express the specific marker, CD90.1. Nuclear staining was
582 performed using DAPI. (B) The axonal connections were observed between multiple RGCs in
583 the merged image.

584 Figure 6. Schematic of the pressure set-up to simulate glaucomatous condition. A sealed
585 pressure chip inside the incubator was connected to a gauge and regulators placed outside by
586 the polyurethane hoses and pneumatic valves via a side opening in the back of incubator.

587 Figure 7. Cell survival assay under NP* and EP** conditions (Two-way ANOVA, N=4, graphs
588 display mean ±SD). (A) There was a significant decrease over time for untreated cells under
589 EP condition with mean difference (Mean Diff.) =45.35, 56, 51.83, 55.43, and 51.2 at 6, 12,
590 24, 36 and 48 hours, respectively ($p<0.0001$). (B) BDNF prevented degeneration of treated
591 RGCs under EP condition with Mean Diff. = 20, 22.52, 23.83, 24, and 26.7 at 6, 12, 24, 36 and
592 48 hours, respectively ($p<0.0001$). (C) RNYK identically protected RGCs under EP condition
593 with Mean Diff. = 26.33, 26.67, 25.67, 26.33, and 27.33 at 6, 12, 24, 36 and 48 hours,
594 respectively ($p<0.0001$).

Figure 1

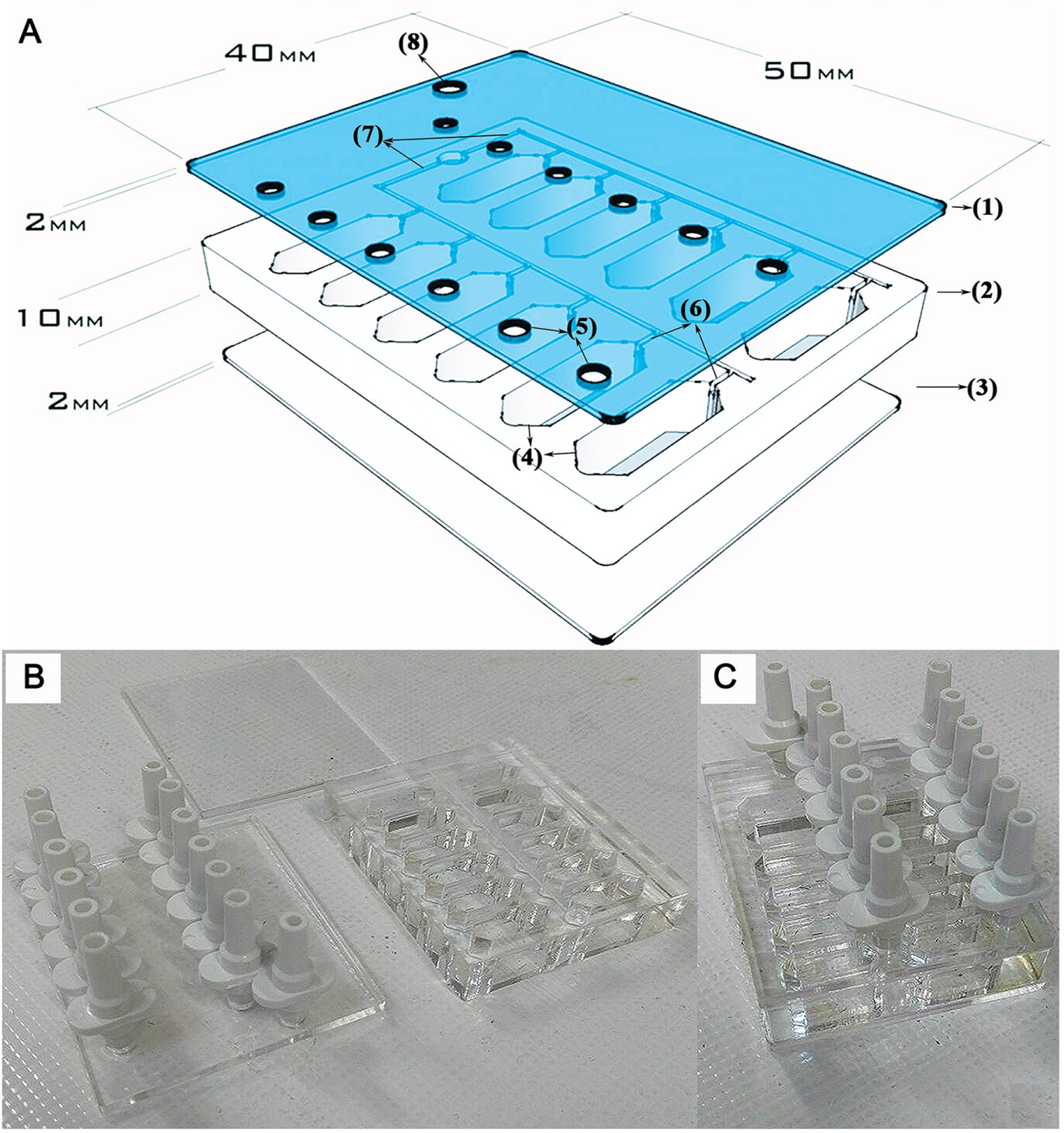

Figure 2

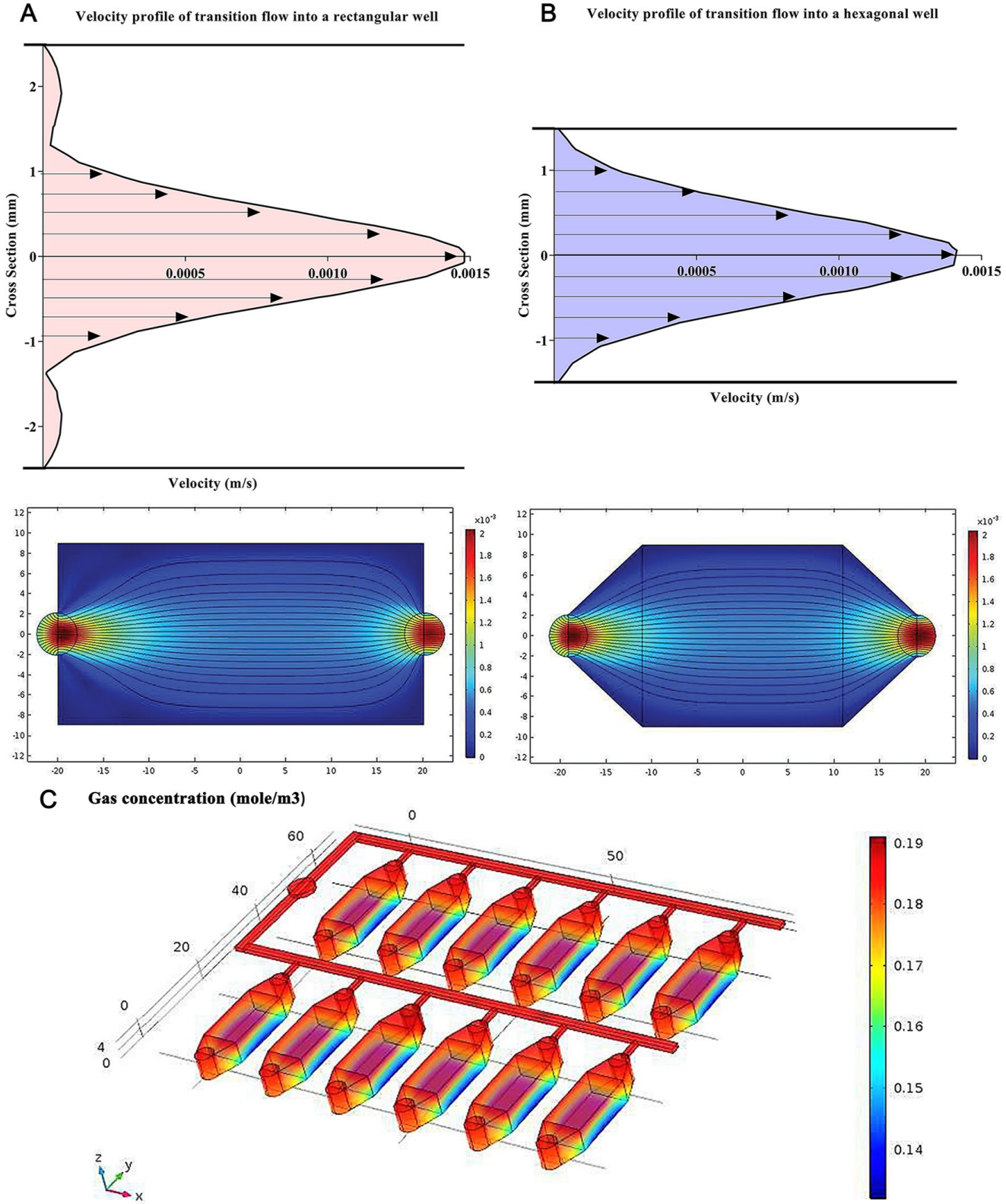
A
Velocity profile of transition flow into a rectangular well
Cross Section (mm)
Velocity (m/s)
0.0005
0.0010
0.0015
B
Velocity profile of transition flow into a hexagonal well
Cross Section (mm)
Velocity (m/s)
0.0005
0.0010
0.0015
C
Gas concentration (mole/m3)
0.19
0.18
0.17
0.16
0.15
0.14

Figure 3

A

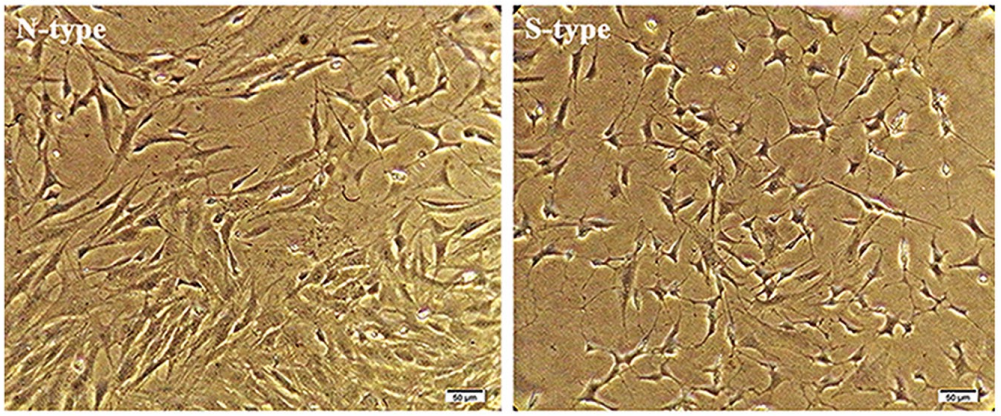
N-type
S-type

B

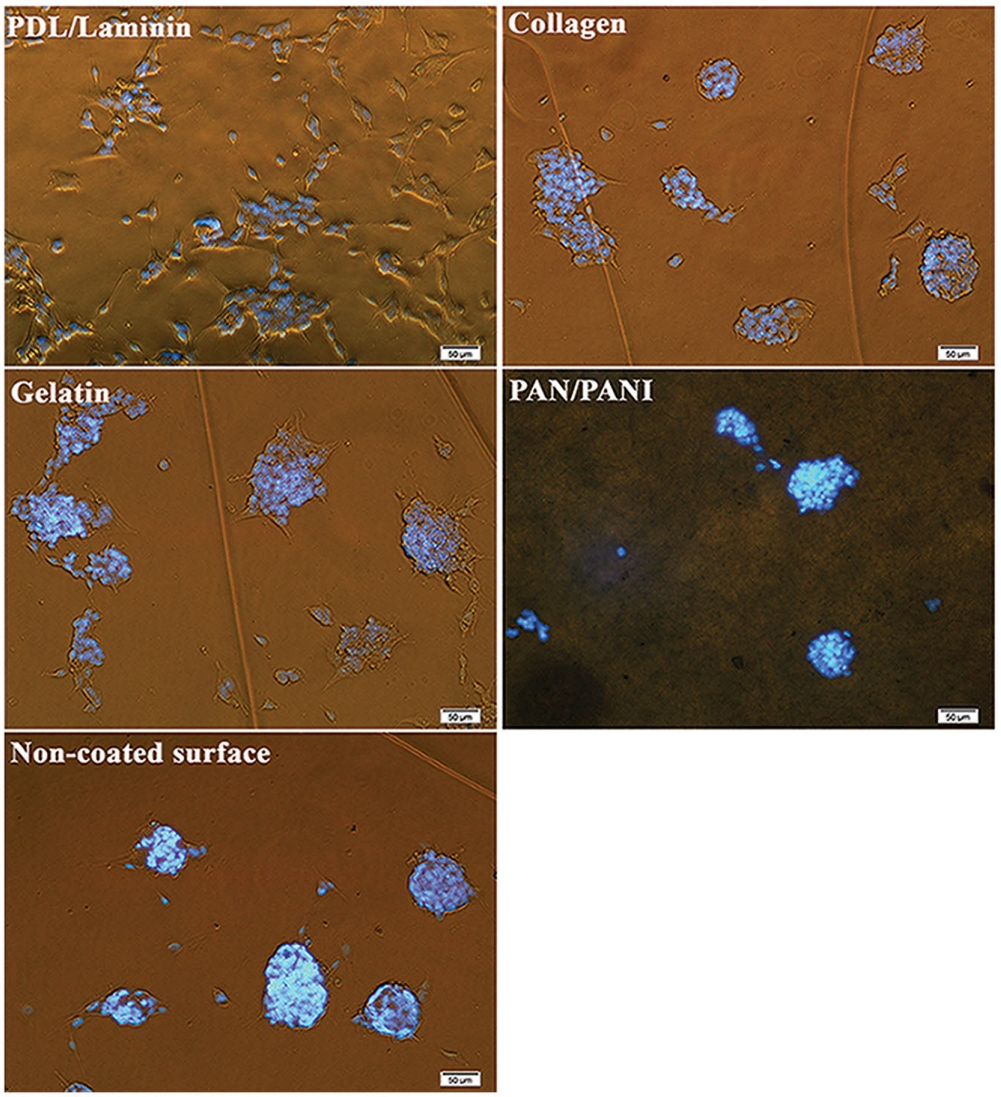
PDL/Laminin
Collagen
Gelatin
PAN/PANI
Non-coated surface

Figure 4

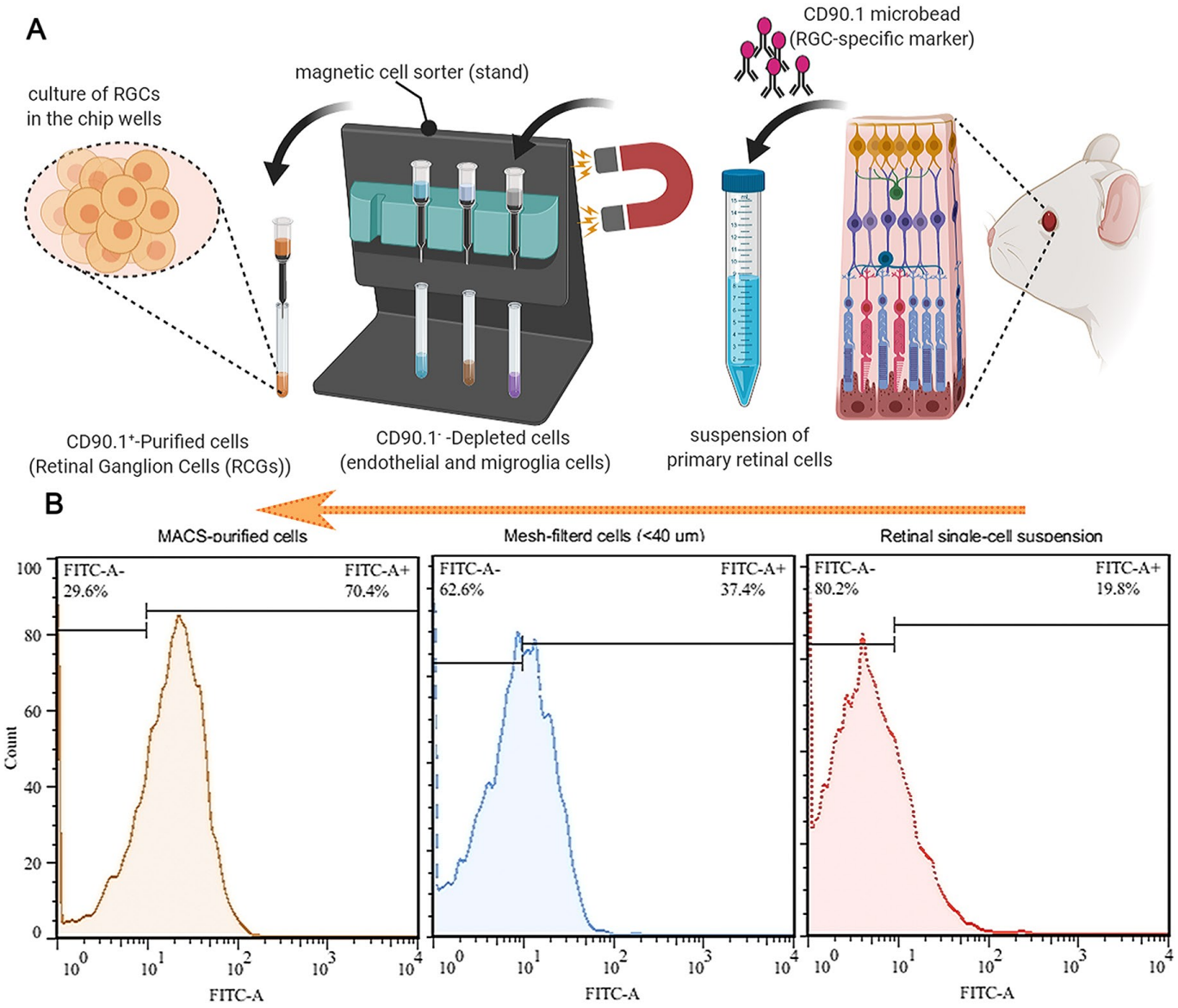
A
CD90.1 microbead
(RGC-specific marker)
magnetic cell sorter (stand)
culture of RGCs
in the chip wells
CD90.1⁺-Purified cells
(Retinal Ganglion Cells (RCGs))
CD90.1⁻ -Depleted cells
(endothelial and migroglia cells)
suspension of
primary retinal cells
B
MACS-purified cells
Mesh-filterd cells (<40 um)
Retinal single-cell suspension
FITC-A-
29.6%
FITC-A+
70.4%
FITC-A-
62.6%
FITC-A+
37.4%
FITC-A-
80.2%
FITC-A+
19.8%
Count
FITC-A

Figure 5

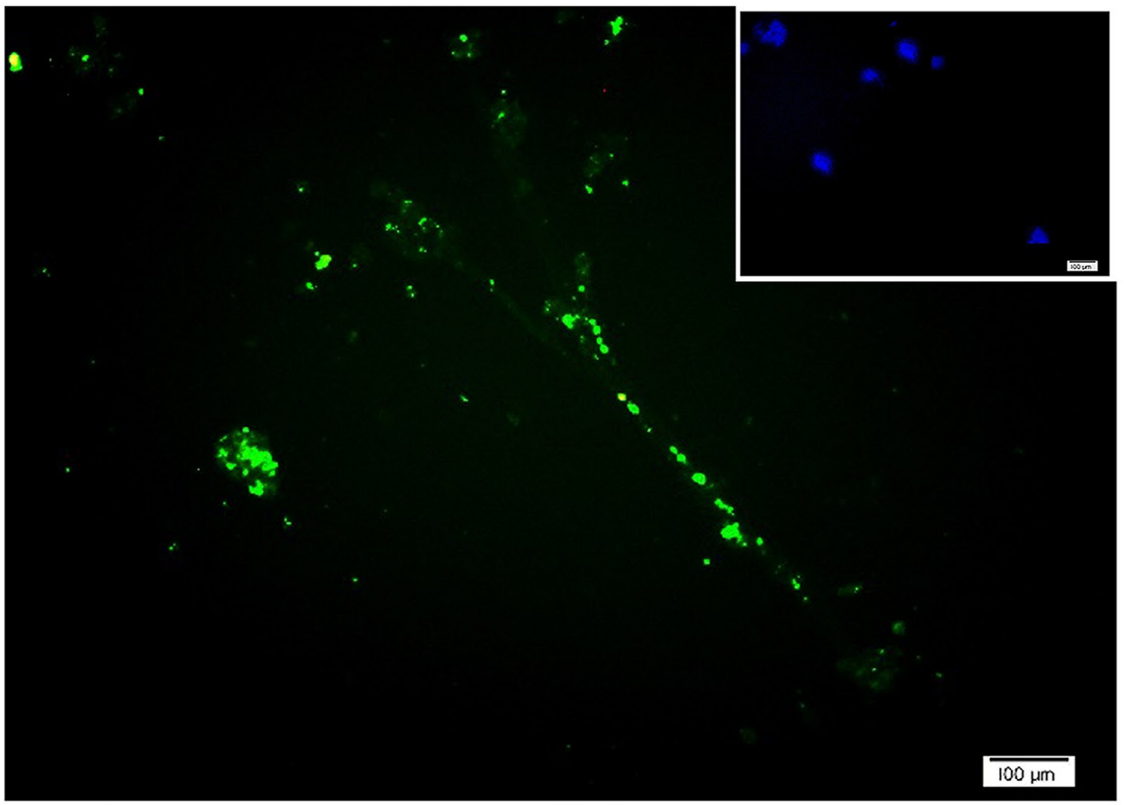

A

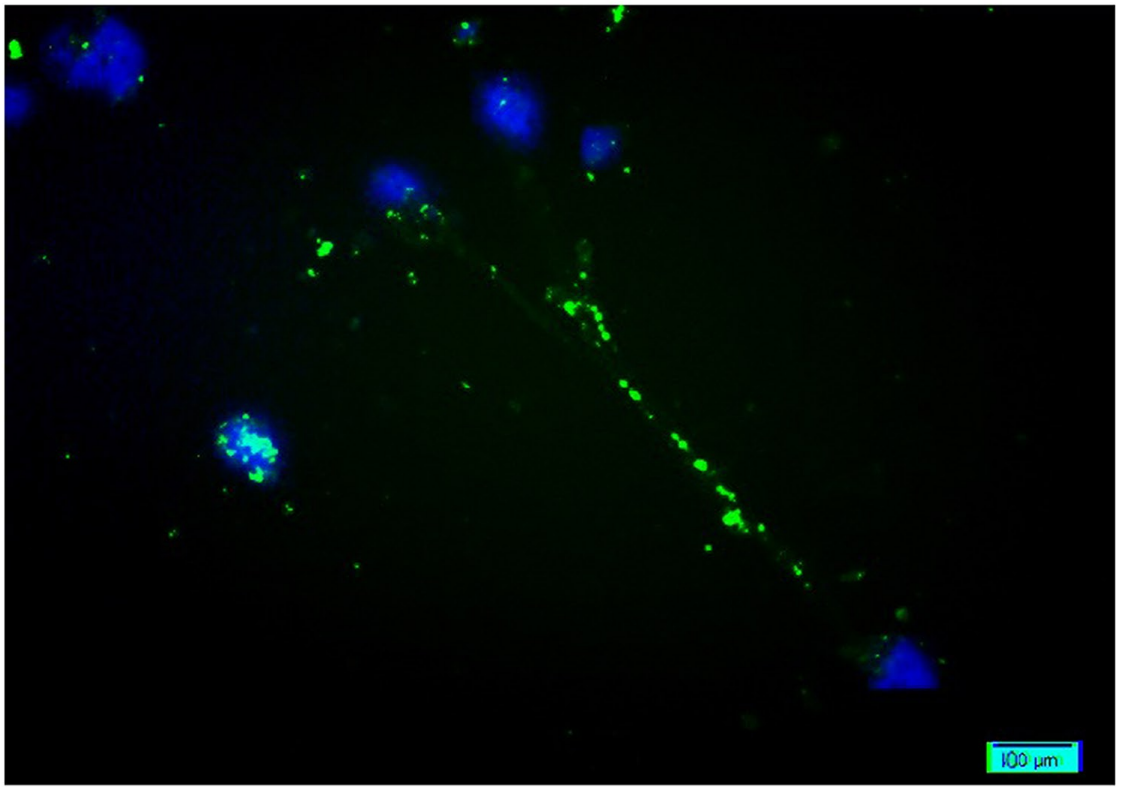

B

Figure 6

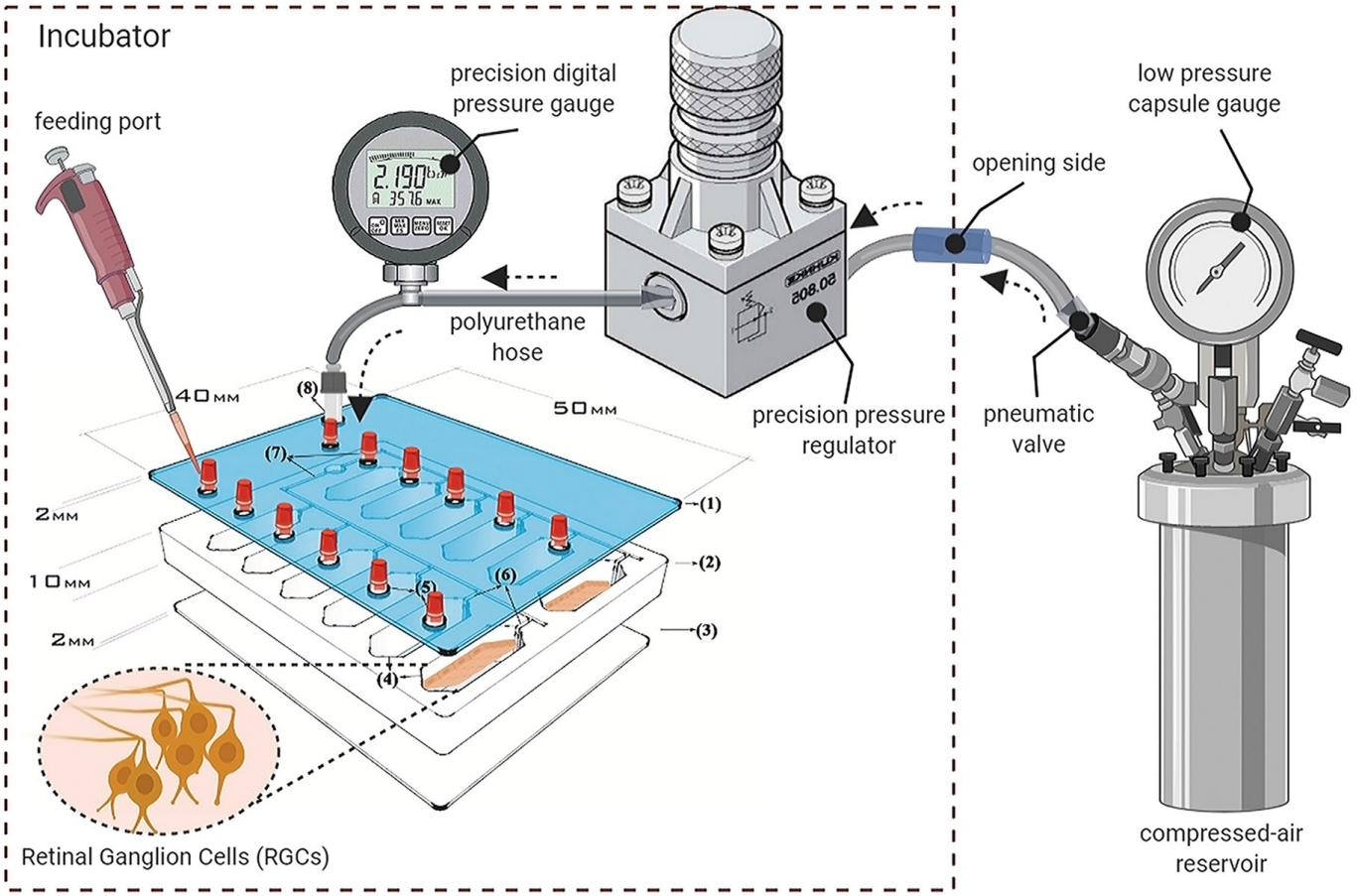
Incubator
feeding port
precision digital pressure gauge
polyurethane hose
precision pressure regulator
opening side
low pressure capsule gauge
pneumatic valve
compressed-air reservoir
40 MM
50 MM
2 MM
10 MM
2 MM
(1)
(2)
(3)
(4)
(5)
(6)
(7)
(8)
Retinal Ganglion Cells (RGCs)

Figure 7

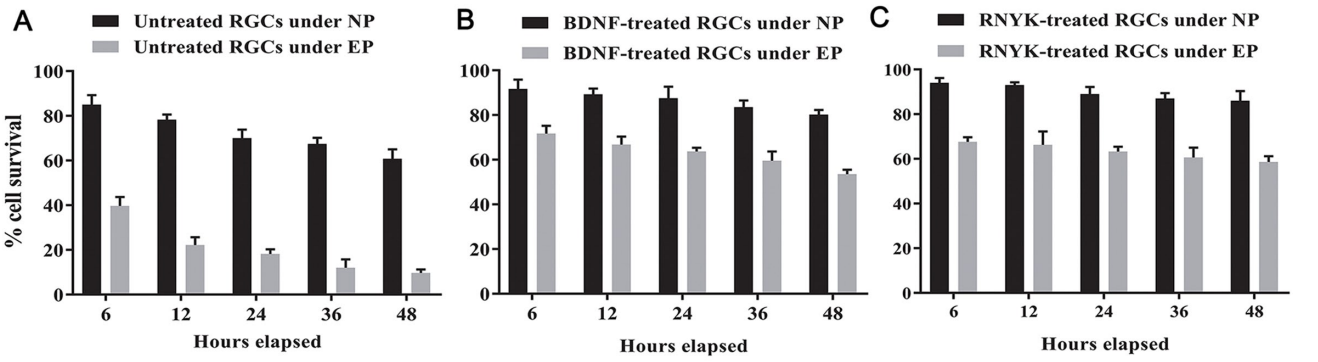
A
Untreated RGCs under NP
Untreated RGCs under EP
% cell survival
100
80
60
40
20
0
6
12
24
36
48
Hours elapsed
B
BDNF-treated RGCs under NP
BDNF-treated RGCs under EP
100
80
60
40
20
0
6
12
24
36
48
Hours elapsed
C
RNYK-treated RGCs under NP
RNYK-treated RGCs under EP
100
80
60
40
20
0
6
12
24
36
48
Hours elapsed